# Volumetric Analysis of Cerebral Hypoperfusion on SPECT: Validation and Reliability

Bernard Infeld, David Binns, Meir Lichtenstein, John L. Hopper and Stephen M. Davis
*Melbourne Neuroscience Center, Departments of Neurology and Nuclear Medicine, Royal Melbourne Hospital, and Department of Public Health and Community Medicine, University of Melbourne, Parkville, Victoria, Australia*

A method of volumetric analysis of hypoperfusion on $^{99m}$Tc-labeled hexamethylpropylene amine oxime SPECT has been developed. This analysis integrates both the size and severity of perfusion reduction, yielding an equivalent volume of cortical tissue having zero blood flow, or the effective hypoperfusion volume. This study aimed to validate the methodology in vitro using the Hoffman brain phantom and two different camera systems, to examine the relationship between spatial resolution and accuracy of volume measurement and to assess the interobserver variability in SPECT studies of stroke patients. **Methods:** Simulated cortical lesions of three different sizes were sequentially incorporated into the Hoffman brain phantom and imaged using both single- and triple-head camera systems. For each system and for each lesion size, successive acquisitions were performed using three progressively larger radii of camera rotation. The hypoperfusion volume for each study was measured three times by a blinded observer, and the percentage difference from the true lesion volume was then calculated. SPECT studies of 32 stroke patients were independently analyzed by two blinded observers. **Results:** At the smallest radii of rotation, mean (s.d.) percentage difference between observed and true volumes was 0.90% (4.80%) for the triple-head and 4.50% (11.58%) for the single-head system. The degree of overestimation was similar for both systems. Percentage overestimation was strongly associated with radius of rotation ($B = 0.71 \pm 0.32$, $p = 0.04$ for the triple-head system; $B = 1.26 \pm 0.55$, $p = 0.03$ for the single-head system) but not with lesion size. The mean difference between hypoperfusion volumes of stroke patients obtained by two observers was 0.045 (3.240) cm$^3$, which was not significant. **Conclusion:** This study has shown that this technique of volumetric analysis of regional hypoperfusion on SPECT is both highly accurate and reproducible between two different camera systems. The degree of overestimation chiefly relates to diminishing spatial resolution. Despite some element of subjectivity, the interobserver variability is negligible.

**Key Words:** SPECT; technetium-99m-labeled hexamethylpropylene amine oxime; computer-assisted image processing; cerebral blood flow; brain phantom

**J Nucl Med 1997; 38:1447–1453**

SPECT of the brain now has an established role in the diagnosis and management of several neurological conditions. These include: seizure focus localization, diagnosis of Alzheimer's disease and other dementias and diagnosis of perfusion changes in cerebrovascular disease (*1,2*). The most readily available radiotracer for studying brain perfusion with SPECT is $^{99m}$Tc-labeled hexamethylpropylene amine oxime (HMPAO). However, unlike PET and $^{133}$Xe studies, which allow direct quantification of regional cerebral blood flow (rCBF), HMPAO SPECT only measures regional counts of activity, which correlate with rCBF.

A variety of semiquantitative methods have been proposed for obtaining a measure of rCBF with SPECT (*3–27*). These methods all normalize the number of counts within a region of interest (ROI), with respect to either global brain activity (*8,9,12,14,25,27*) or the activity within a reference region that is believed to be unaffected by the disease under study (*3–7,10,12,13,15–24,26,27*). These techniques differ by the number of slices analyzed, the method of delineation of pathology or the normalization algorithm. There is no standardized or validated method of semiquantitative analysis, and this disparity makes comparison of studies difficult.

Only a few methods for volumetric analysis of cerebral hypoperfusion have been proposed (*3,28,29*), and none have been validated in vitro. Image degradation and distortion due to photon attenuation and scatter, inadequate spatial resolution and partial volume effects are the major limitations to accurate quantitation.

The aim of this study was to develop a method of volumetrically evaluating cerebral hypoperfusion on SPECT HMPAO scans. This method, a modification of the technique of Mountz (*28*), integrates both the size and severity of perfusion reduction and produces a volume measure (in cm$^3$) equivalent to a hypothetical volume of cortical tissue with zero perfusion, or an effective hypoperfusion volume. We then aimed to validate this technique in vitro using a brain phantom and two different camera systems, to analyze the effect of spatial resolution on its accuracy and to examine its interobserver variability in stroke patients.

## MATERIALS AND METHODS

### Volumetric Quantitation Algorithm

The principle of this method is to determine the number of counts lost from the affected cerebral region compared with the homologous unaffected contralateral region. This is then converted into an equivalent volume of cortex having zero count activity by using the count value of a normal cortical voxel and the tissue volume corresponding to a voxel.

Using a computerized video display, all involved transaxial cerebral slices are initially visually identified. Then, for each involved slice, using a cursor system, ROIs are manually drawn to outline a homologous region in the normal hemisphere, approximating the affected region. The "normal" ROI is constructed so as to include all pixels having visually apparent greater count values than homologous pixels in the affected hemisphere. To ensure inclusion of all affected pixels, a perimeter of normal brain tissue 1–2 pixels beyond the perceived lesion margins is also included in the ROI. The normal ROI is then mirrored onto the affected hemisphere and symmetrically placed to include the entire region of hypoperfusion (Fig. 1). Total counts are then obtained from the normal and lesion ROIs for all involved slices and summed to produce total normal and total lesion counts, respectively.

A normalized voxel count (NVC), the count value of a normal cortical voxel, is then obtained from the brain count histogram.

Received Jul. 11, 1996; revision accepted Feb. 19, 1997.
For correspondence or reprints contact: Stephen M. Davis, MD, FRACP, Department of Neurology, c/o Post Office, Royal Melbourne Hospital, Victoria 3050, Australia.

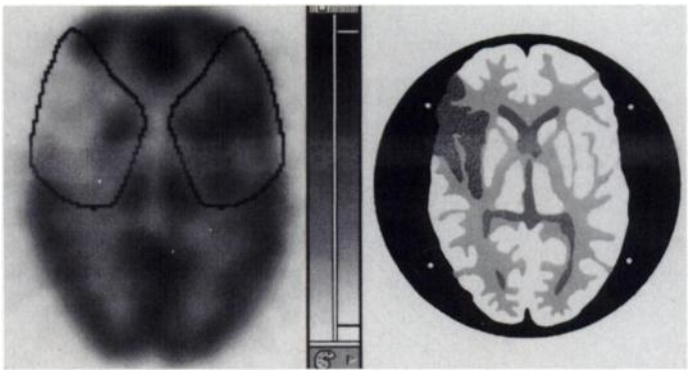

**FIGURE 1.** Gray-scale SPECT image (left) and a corresponding slice of the Hoffman brain phantom (right) with a simulated perfusion defect. Symmetric regions of interest encompass the affected and homologous contralateral areas. The different structures of the Hoffman phantom have been schematically colored. Black = bone and scalp; white = gray matter; light gray = white matter; dark gray = ventricles; mottled gray = artificial lesion.

This is a plot of the frequency of all voxel count values within all cerebral slices of the brain image. A typical brain count histogram is illustrated in Figure 2. The NVC is determined by the x-intercept of the extrapolated linear fit applied to the down-sloping portion of the histogram (Fig. 2).

The total volume of regional hypoperfusion is then calculated using the formula:

$$\text{hypoperfusion volume} = \frac{\text{normal counts} - \text{lesion counts}}{\text{NVC}} \times \text{voxel volume},$$

where the voxel volume is obtained from supplied proprietary software.

### Validation

Several artificial cortical "lesions" of various sizes were simulated for the three-dimensional Hoffman brain phantom (*30,31*) using a nonporous, hydrophobic silicone polymer (Fig. 1). These lesions were sequentially incorporated into the phantom for imaging. The composite lesion phantom was filled with water containing 200 mBq of $^{99m}$Tc. SPECT imaging was performed using two different gamma camera systems: a single-headed GE 400AC Starcam and a triple-headed Siemens Multispect (MS3). The true volume of each silicone lesion was determined by immersion in a water bath and measuring the volume of water displaced.

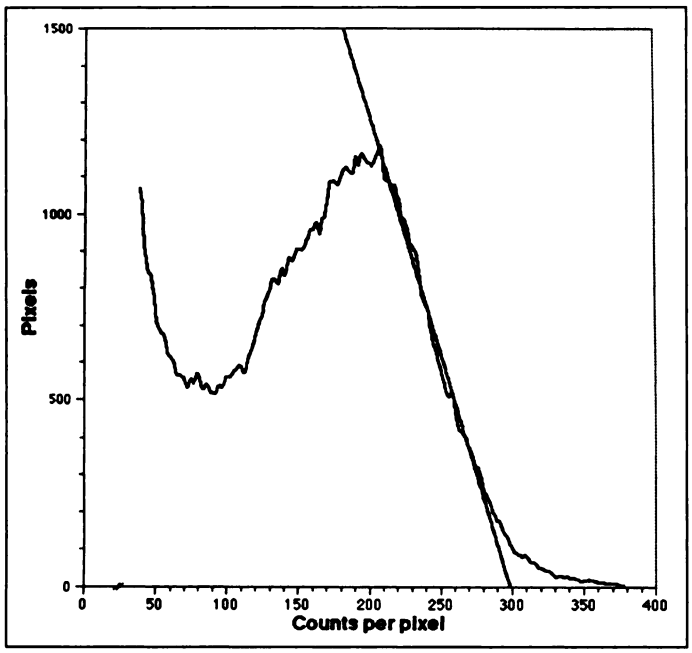


**FIGURE 2.** Brain count histogram showing derivation of the NVC. A linear fit is applied to the down-sloping portion following the cortical peak and is extrapolated to the x-axis. The NVC is the count value of the x-intercept.

To examine the effects of diminishing spatial resolution on the accuracy of volumetric analysis, each lesion phantom was imaged three times using radii of rotation of 12.9, 16.9 and 20.9 cm, respectively, for the MS3 system; and 14.4, 19.0 and 23.3 cm, respectively, for the GE400 system. Spatial resolution for each system was analyzed by acquiring a point source in air at each radius of rotation.

### SPECT Methodology

SPECT acquisition and processing parameters reflected our clinical protocol. Higher count rates were achieved from phantom studies compared to clinical studies. However, total acquisition times were adjusted to achieve 2.5–3 times the average total counts from clinical studies. No scatter correction was applied.

On both systems, a 20% asymmetric window was centered 5% above the 140-keV photon peak. All SPECT studies were obtained with high-resolution parallel-hole collimators through a circular arc of 360°. On the MS3, a total of 96 frames of 128 × 128 word data were acquired with a zoom factor of 1.45. Studies acquired on the GE400 system included 64 frames with no zoom applied.

Tomographic reconstruction performed on both systems used the filtered backprojection technique. Chang's first-order attenuation correction was applied using an attenuation coefficient of 0.12 $cm^{-1}$. Prefiltering on the MS3 incorporated a Shepp–Logan–Hanning (*32*) filter with a cutoff frequency of 0.65 cycles/cm. A postreconstruction zoom value of 1.6 was applied. Two-pixel-deep, 128 × 128 word transaxial slices were used for analysis. On the GE400, a Butterworth prefilter with a Nyquist frequency of 0.4 cycles/cm and a slope of 10 was used. Two-pixel deep, 64 × 64 word transaxial slices were used for analysis.

The voxel volume for each imaging system was obtained from supplied proprietary software and verified using a point-source phantom. The respective voxel volumes were 10.23 $mm^3$ for the MS3 system and 64.00 $mm^3$ for the GE400 system.

Using the volumetric method already described, each lesion study was analyzed by a blinded observer three times to obtain three values for the observed lesion volume at each level of resolution. For each observed value, the percentage difference between the observed and true volumes was calculated and expressed as a percentage of the mean of the observed and true volumes, as follows:

$$\text{percentage difference} = \frac{\text{observed volume} - \text{true volume}}{\text{observed volume} + \text{true volume}} \times 200\%.$$

To study the combined effects of attenuation, scatter and partial voluming and to verify our choice of NVC, additional image acquisitions were performed of the composite lesion phantom with the 10 uppermost brain slices removed. This effectively divided the phantom into "brain" and cylindrical portions each having equal concentration of radioactivity. Separate histograms were generated for each portion (Fig. 3), and the lesion volume was calculated using different NVCs each obtained from defined parts of either histogram.

### Interobserver Variability

Cerebral hypoperfusion volumes in 32 stroke patients were measured by two blinded, independent observers. These patient studies were randomly chosen from a series of patients with middle cerebral territory cortical infarction undergoing SPECT scans, as previously described (*33*). For each patient study, the interobserver

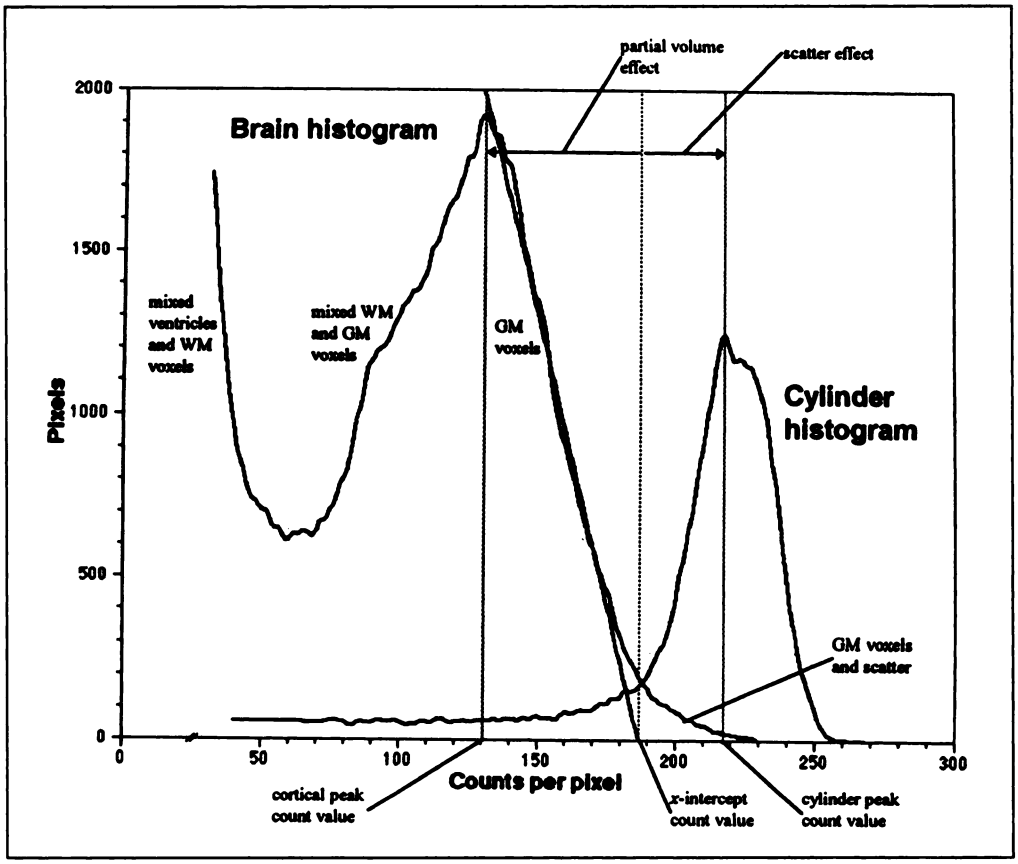


**FIGURE 3.** Brain count histograms for the brain and cylindrical portions of the Hoffman phantom. An extrapolated linear fit has been applied to the brain histogram to obtain the NVC. The regions of the brain image contributing to the different parts of the brain histogram are indicated. The cortical peak is shifted leftward relative to the x-intercept count value due to the partial volume effect. The cylinder peak is shifted right relative to the x-intercept count value because of the effect of photon scatter. In a perfect camera system, these three count values would coincide. WM = white matter; GM = gray matter.

variability was calculated as the difference between the two observers' measurements.

### Statistical Analysis

Student's t-test was used to test for differences in mean percentage overestimation between the two camera systems. The effects of radius of rotation and lesion size on percentage overestimation of hypoperfusion volume estimation were evaluated using linear regression. Multivariate linear regression was used to assess whether the percentage overestimation was independently associated with radius of rotation and/or lesion size. The regression coefficient, B, its s.e. and nominal p-value are presented. Differences in observed hypoperfusion volumes between the two observers were assessed using paired Student's t-test. Findings were considered not significant if the nominal p-value was greater than 0.05.

## RESULTS

The effect of radius of rotation on spatial resolution for each system is shown in Table 1. Mean observed volumes and respective percentage differences from true volumes for each lesion at each level of resolution are shown in Table 2 for the MS3 imaging system and Table 3 for the GE400. The overall mean (s.d.) percentage overestimation for the MS3 system was 4.36% (5.89%; 95% confidence interval, 2.03%–6.70%), whereas that for the GE400 system was 8.71% (11.14%; 4.30%–13.12%). At the minimum radii of rotation, mean percentage difference between observed and true volumes was 0.90% (4.80%; −2.79%–4.59%) for the MS3, 4.50% (11.58%; −4.40%–13.40%) for the GE400 and 2.70% (8.79%; −1.67%–7.07%) for both systems combined. Furthermore, at the minimum radii of rotation, there was no significant difference in the degree of overestimation between the two systems.

The relationships between percentage overestimation and both radius of rotation and lesion size are shown in Figures 4 and 5 for each imaging system. For the MS3 system, percentage overestimation of volume measurement was strongly associated with radius of rotation ($B = 0.71 \pm 0.32$; $p = 0.04$) but not with lesion size ($B = 0.20 \pm 0.14$; $p = 0.2$). In a multivariate analysis, only radius of rotation was an independent determinant of percentage overestimation ($B = 0.71 \pm 0.31$; $p = 0.03$). Similarly, for the GE400 system, percentage overestimation was associated with radius of rotation ($B = 1.26 \pm 0.55$; $p = 0.03$) but only weakly with lesion size ($B = 0.45 \pm 0.25$; $p = 0.09$). These relationships remained unchanged after multivar-

**TABLE 1**
Relationship between Radius of Rotation and Spatial Resolution for Both Camera Systems

| Camera | Radius of rotation (cm) | SPECT resolution (mm) |
|---|---|---|
| MS3 | 12.9 | 7.13 |
| | 16.9 | 8.48 |
| | 20.9 | 10.81 |
| GE400 | 14.4 | 11.0 |
| | 19.0 | 13.9 |
| | 23.3 | 15.9 |

The resolution values were derived from the FWHM of the point spread function in air.

**TABLE 2**
Mean Observed Volumes and Respective Mean Percentage Differences from True Lesion Volume for the MS3 System at Each Level of Resolution

| Lesion no. | True volume ($cm^3$) | Radius of rotation (cm) | Mean observed volume (s.d.) ($cm^3$) | Mean percentage difference (s.d.) (%) |
|---|---|---|---|---|
| 1 | 24.11 | 12.9 | 24.40 (0.49) | 1.19 (2.01) |
| | | 16.9 | 25.01 (0.64) | 3.67 (2.56) |
| | | 20.9 | 28.15 (1.14) | 15.42 (3.96) |
| 2 | 8.74 | 12.9 | 8.36 (0.03) | −4.43 (0.32) |
| | | 16.9 | 9.53 (0.11) | 8.62 (1.14) |
| | | 20.9 | 9.15 (0.31) | 4.58 (3.44) |
| 3 | 5.56 | 12.9 | 5.90 (0.16) | 5.94 (2.66) |
| | | 16.9 | 5.82 (0.25) | 4.52 (4.20) |
| | | 20.9 | 5.55 (0.17) | −0.22 (3.11) |

iate analysis (B = 1.26 ± 0.52; p = 0.02 and B = 0.45 ± 0.23; p = 0.07, respectively).

We then further verified our choice of NVC, using the phantom divided into brain and cylindrical sections. Lesion volumes for this image set were calculated using four different possible NVCs. These were the x-intercept of the line fitted to the brain histogram, the average count value of the normal regions (*28*), the peak of the brain histogram (*29,33*) and the peak of the cylinder histogram (Fig. 3). The respective calculated lesion volumes and percentage differences from the true lesion volume for both imaging systems are shown in Table 4.

Differences in hypoperfusion volumes of the group of stroke patients between two observers are shown in Figure 6. The mean (s.d.) difference in hypoperfusion volumes between the two observers was 0.045 (3.240) $cm^3$. This difference was not statistically significant.

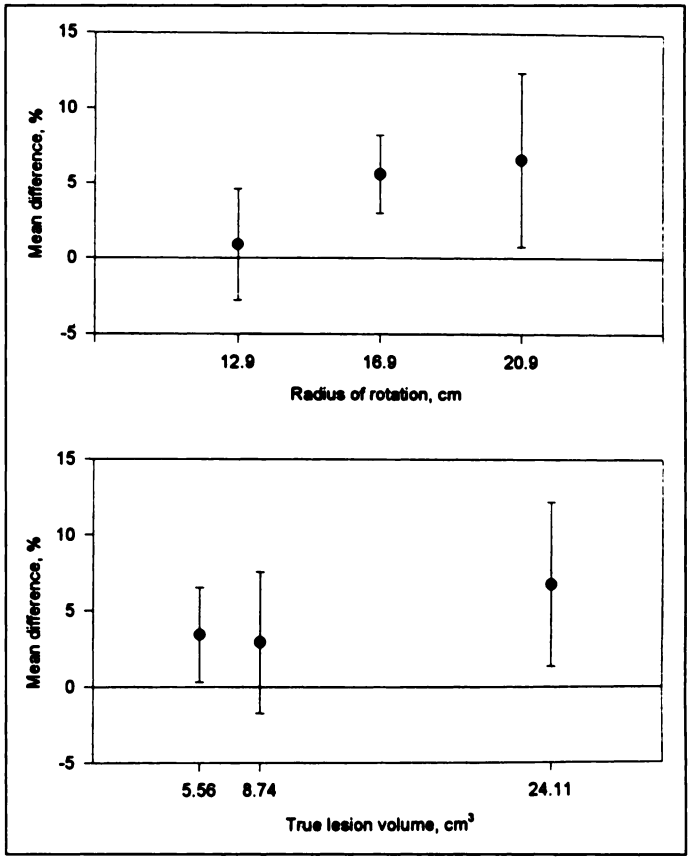


**FIGURE 4.** The relationship between mean percentage difference between observed and true lesion volumes and radius of rotation (upper) and lesion size (lower) for the MS3 imaging system. Error bars denote 95% confidence intervals.

## DISCUSSION

This study has described a technique for volumetrically analyzing hypoperfusion on HMPAO SPECT brain images. We have demonstrated in vitro, using the Hoffman brain phantom with artificially simulated lesions, that measured volumes are reasonably accurate and reproducible between two different SPECT camera systems. Although this technique tends to overestimate lesion volumes, the degree of overestimation chiefly relates to the radius of camera rotation, which in turn affects spatial resolution, and is independent of lesion volume. In fact, at the minimum rotation radii used in clinical practice for both camera systems, the percentage overestimation was not significantly different from zero.

**TABLE 3**
Mean Observed Volumes and Respective Mean Percentage Differences from True Lesion Volume for the GE400 System at Each Level of Resolution

| Lesion no. | True volume ($cm^3$) | Radius of rotation (cm) | Mean observed volume (s.d.) ($cm^3$) | Mean percentage difference (s.d.) (%) |
|---|---|---|---|---|
| 1 | 24.11 | 14.4 | 28.81 (1.00) | 17.72 (3.43) |
| | | 19.0 | 28.01 (0.25) | 14.99 (0.89) |
| | | 23.3 | 25.87 (2.08) | 6.84 (7.91) |
| 2 | 8.74 | 14.4 | 8.98 (0.32) | 2.66 (3.58) |
| | | 19.0 | 9.34 (0.35) | 6.62 (3.66) |
| | | 23.3 | 10.89 (1.19) | 21.50 (10.45) |
| 3 | 5.56 | 14.4 | 5.20 (0.37) | −6.89 (7.04) |
| | | 19.0 | 5.34 (0.42) | −4.27 (7.92) |
| | | 23.3 | 6.74 (0.26) | 19.21 (3.87) |

Several aspects of our technique require explanation. These are the methods of drawing ROIs and of obtaining the NVC value. The rationale of our approach was to try to compensate for the combined degrading effects of photon scatter and partial voluming on both the SPECT image and the distribution of pixel count values in the brain count histogram. These combined effects cause a reduction of count density in high-activity regions, such as cortex and other gray matter, while increasing count density in regions having low activity, such as white matter, ventricles and perfusion defects (*34–36*). Hence, contrast between gray matter, white matter and perfusion defects is reduced. Edges of perfusion defects are blurred, causing them to appear larger. It is important, then, to include all asymmetric pixels in the drawn ROIs, as we have done, as this will ensure that the total count loss of the perfusion defect is properly determined. ROIs are first drawn on the normal, homologous hemisphere because the distinction between the perfusion defect and the overlying scalp is often not apparent.

The next important step is to estimate as accurately as possible the count value of a normal cortical voxel, the NVC. This is obtained from the brain count histogram, but the effects of photon scatter and partial voluming again need to be considered. Figure 3 shows the count histograms derived from the brain (left) and cylinder (right) phantoms, each having the same diameter and equal concentrations of radioactivity. The partial volume effect is particularly important (*37*) because the cerebral cortex is a complex structure less than 5 mm thick (*38*) and is, therefore, well below the spatial resolution of current SPECT systems (*1*). Compared with the results that would be obtained using an ideal camera system, partial voluming of the cerebral cortex causes the cortical portion of the brain histo-

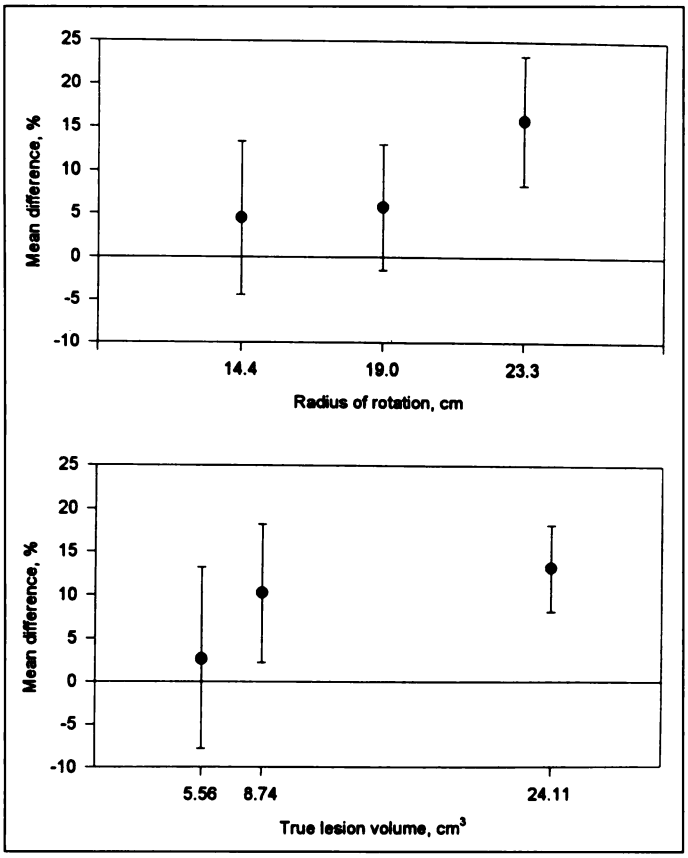


**FIGURE 5.** The relationship between mean percentage difference between observed and true lesion volumes and radius of rotation (upper) and lesion size (lower) for the GE400 imaging system. Error bars denote 95% confidence intervals.

gram to be shifted towards the left. In addition, statistical variation causes broadening of the cortical histogram, but this is asymmetrical (broader on the left side of the peak) because of partial voluming. In contrast, the narrower histogram of the cylinder phantom is shifted to the right due to the effect of photon scatter. Photon scatter also accounts for the rightmost "tail" of the cortical histogram because this lies well beneath the peak of the cylinder histogram. The true count value of a normal cortical voxel probably lies between the peaks of the two histograms. This value can be reasonably estimated by applying a line of best fit to the linear portion of the down-sloping part of the cortical histogram and extrapolating it to obtain its x-intercept value.

**TABLE 4**
Mean Volumes and Percentage Differences from the True Lesion Volume for Each Method of Obtaining the NVC

| Camera | Method | Mean observed volume (s.d.) ($cm^3$) | Mean percentage difference (s.d.) (%) |
|---|---|---|---|
| MS3 | x-intercept | 15.01 (0.03) | −4.50 (0.18) |
| | Mean count | 20.83 (0.19) | 28.13 (0.89) |
| | Peak count | 21.01 (0.04) | 28.95 (0.17) |
| | Cylinder peak | 12.64 (0.02) | −21.54 (0.17) |
| GE400 | x-intercept | 16.34 (0.61) | 3.99 (3.69) |
| | Mean count | 22.27 (1.28) | 34.50 (5.47) |
| | Peak count | 22.11 (0.82) | 33.89 (3.58) |
| | Cylinder peak | 12.43 (0.46) | −23.29 (3.65) |

The true lesion volume was 15.70 $cm^3$.

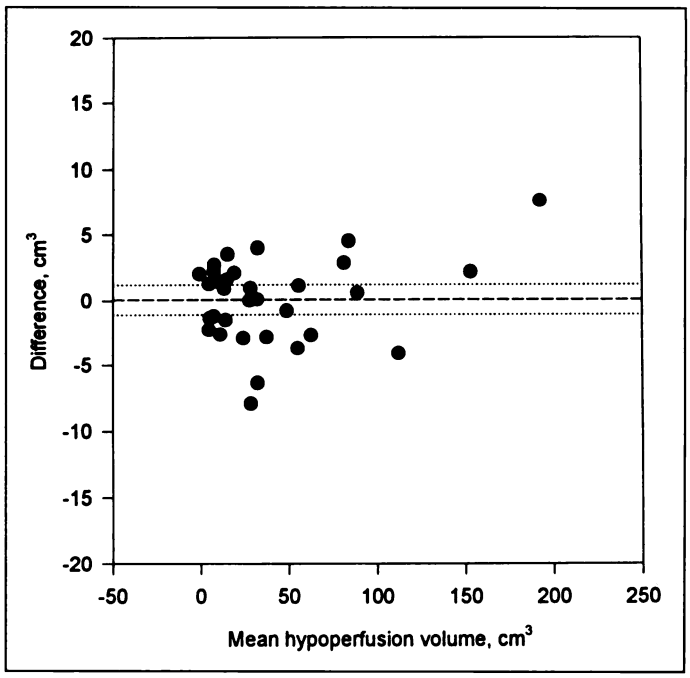


**FIGURE 6.** Interobserver variability. Differences in hypoperfusion volumes between two observers as a function of the mean. Dashed and dotted lines mark overall mean difference and 95% confidence intervals, respectively.

It must be emphasized, however, that there is no mathematical basis for this approach. In fact, we had initially assumed that the peak value of the brain histogram (the most frequently occurring or mode count value) would equate with the count value of a normal cortical voxel (*29,33*). Similarly, Mountz (*28*) used the average count value of the normal homologous regions (total counts/number of pixels). During these experiments with the Hoffman phantom, we unexpectedly found that using either of these methods caused lesion volumes to be overestimated by around 30% (Table 4). We hypothesized that these errors were due to the partial volume effect. The x-intercept method is an approximate means of obtaining the true NVC, simultaneously correcting for the partial volume effect and allowing for photon scatter. Although purely empirical, this technique nevertheless appears to be supported by our experimental results.

We chose the Hoffman brain phantom to validate our methodology because we wanted to simulate photon scatter, attenuation and partial volume effects present in routine clinical brain imaging (*35*). By imaging the phantom using increasing radii of camera rotation, we were able to demonstrate a linear relation between spatial resolution and accuracy of volume measurement. The Hoffman brain phantom was derived from T1-weighted magnetic resonance imaging structural data of one normal volunteer (*30,31*). It has previously been shown that the Hoffman phantom is useful in assessing the accuracy of PET data (*31*). Other factors causing image degradation, such as patient movement and poor radiolabeling, although often encountered, would be difficult to simulate using this model. On the other hand, cylinder-type phantoms yield images that are totally disparate with in vivo studies and, as shown in this study, do not recreate the physical effects of in vivo imaging.

One of the limitations of our volumetric method is that it assumes that a focal brain lesion exclusively occupies gray matter, and it effectively measures an equivalent theoretical volume of cortex having zero blood flow. Most focal pathological processes, such as cortical infarction or tumor, often involve adjacent white matter. The white matter contribution

would be ascribed to a smaller gray matter component of about one-quarter the true size. Nonetheless, blood flow in the cerebral cortex is between 2 and 5 times that of white matter (*20,39–43*), reflecting greater metabolic demands. Hence, the effect of focal pathology on perfusion is much greater in the cortex than in white matter. In substantial cerebral lesions, therefore, the degree of white matter involvement is proportional to the gray matter component. We have previously found a significant correlation between hypoperfusion volume and infarct volume on CT scan in patients with chronic cortical infarction (after luxury perfusion has abated) (*44*). In validating our methodology, we were unable to model lesions involving white matter in the Hoffman phantom for technical reasons relating to the narrow spacing (0.6 mm) between the layers of lucite making up its white matter structure (*30*). Our intention, however, was to simulate problems of image degradation, not in vivo pathology.

It should be stressed that our volumetric algorithm is essentially semiquantitative in nature and is not intended to represent an exact quantitation of either tissue damage or rCBF. Furthermore, like most other semiquantitative methods (*3–5,7,10,13,15,17–24,26–28*), it assumes that rCBF is normally symmetric between homologous regions. Although significant side-to-side differences in rCBF have been found in normal volunteers, they only range from 0% to 3% (*20,40,43,45,46*). Therefore, normal side-to-side asymmetry constitutes a negligible error when hypoperfusion volumes are measured in patients.

There is a significant element of subjectivity in our method. The identification of perfusion deficits within all affected brain slices and the manual drawing of ROIs both require a degree of interpretation on the part of the operator. Nevertheless, the interobserver variability in our study was not statistically significant. This reflects reasonable consistency between observers in drawing ROIs.

Our technique is only applicable to unilateral disease processes, such as stroke, tumors and focal epilepsy. We have found this methodology particularly suited to the serial evaluation of acute interventional therapies, such as thrombolysis, in patients with middle cerebral territory cortical infarction. Measured hypoperfusion volumes can also be readily correlated with neurological and functional scores (*29*), remote effects such as crossed cerebellar diaschisis (*33*) and other imaging modalities (*28,29,33*). Hypoperfusion volume measurement represents a theoretical construct rather than an exact quantitation of rCBF, but it is a robust and clinically useful technique for evaluation of focal brain disorders.

## CONCLUSION

We have developed a method to volumetrically analyze regional hypoperfusion on SPECT. This analysis integrates both the size and severity of perfusion reduction, yielding an equivalent volume of cortical tissue having zero blood flow. Using a Hoffman brain phantom fitted with different-sized simulated lesions, we have shown that this method is robust, accurate and reproducible between two different camera systems. The degree of overestimation relates chiefly to diminishing spatial resolution rather than to lesion size.

We have explored the interobserver variability of this technique by comparing the observed hypoperfusion volumes in a group of stroke patients between two independent observers. Despite the subjectivity involved in manually drawing ROIs, the interobserver variability is negligible.

Volumetric analysis is readily applicable to the study of focal brain pathologies, such as stroke, epilepsy and brain tumors. It facilitates early diagnostic and prognostic information, comparison with other imaging modalities such as CT or magnetic resonance imaging, correlation with clinical measurements and monitoring effects of therapy.

## ACKNOWLEDGMENTS

This work is supported by grants from the National Health and Medical Research Council (Australia) and the Australian Stroke and Neuroscience Institute. We thank the Department of Nuclear Medicine, Austin Hospital, Melbourne, for the loan of the Hoffman phantom and Ian Larson (Department of Chemistry, University of Melbourne) for his technical assistance.

## REFERENCES

1. Holman BL, Devous MD Sr. Functional brain SPECT: the emergence of a powerful clinical method. *J Nucl Med* 1992;33:1888–1904.
2. Davis SM. Single-photon emission computed tomography. In: Kelley RE, ed. *Functional neuroimaging*. Armonk, NY: Futura Publishing Company; 1994:51–68.
3. Baird AE, Donnan GA, Austin MC, Fitt GJ, Davis SM, McKay WJ. Reperfusion after thrombolytic therapy in ischemic stroke measured by single-photon emission computed tomography. *Stroke* 1994;25:79–85.
4. Defer G, Moretti JL, Cesaro P, Sergent A, Raynaud C, Degos JD. Early and delayed SPECT using *N*-isopropyl *p*-iodoamphetamine iodine 123 in cerebral ischemia. A prognostic index for clinical recovery. *Arch Neurol* 1987;44:715–718.
5. Giubilei F, Lenzi GL, Di Piero V, et al. Predictive value of brain perfusion single-photon emission computed tomography in acute ischemic stroke. *Stroke* 1990;21:895–900.
6. Goulding P, Burjan A, Smith R, et al. Semi-automatic quantification of regional cerebral perfusion in primary degenerative dementia using $^{99m}$Tc-hexamethylpropylene amine oxime and single-photon emission tomography. *Eur J Nucl Med* 1990;17:77–82.
7. Hanson SK, Grotta JC, Rhoades H, et al. Value of single-photon emission computed tomography in acute stroke therapeutic trials. *Stroke* 1993;24:1322–1329.
8. Hellman RS, Tikofsky RS, Collier BD, et al. Alzheimer's disease: quantitative analysis of $^{123}$I-iodoamphetamine SPECT brain imaging. *Radiology* 1989;172:183–188.
9. Hooper HR, McEwan AJ, Lentle BC, Kotchon TL, Hooper PM. Interactive three-dimensional region of interest analysis of HMPAO SPECT brain studies. *J Nucl Med* 1990;31:2046–2051.
10. Jagust WJ, Reed BR, Seab JP, Budinger TF. Alzheimer's disease. Age at onset and single-photon emission computed tomographic patterns of regional cerebral blood flow. *Arch Neurol* 1990;47:628–633.
11. Johnson KA, Holman BL, Mueller SP, et al. Single-photon emission computed tomography in Alzheimer's disease. Abnormal iofetamine $^{123}$I uptake reflects dementia severity. *Arch Neurol* 1988;45:392–396.
12. Karbe H, Kertesz A, Davis J, Kemp BJ, Prato FS, Nicholson RL. Quantification of functional deficit in Alzheimer's disease using a computer-assisted mapping program for $^{99m}$Tc-HMPAO SPECT. *Neuroradiology* 1994;36:1–6.
13. Lee RG, Hill TC, Holman BL, Royal HD, O'Leary DH, Clouse ME. Predictive value of perfusion defect size using N-isopropyl-(I-123)-p-iodoamphetamine emission tomography in acute stroke. *J Neurosurg* 1984;61:449–452.
14. Maurer AH, Siegel JA, Comerota AJ, Morgan WA, Johnson MH. SPECT quantification of cerebral ischemia before and after carotid endarterectomy. *J Nucl Med* 1990;31:1412–1420.
15. Montaldi D, Brooks DN, McColl JH, et al. Measurements of regional cerebral blood flow and cognitive performance in Alzheimer's disease. *J Neurol Neurosurg Psychiatry* 1990;53:33–38.
16. O'Mahony D, Coffey J, Murphy J, et al. The discriminant value of semiquantitative SPECT data in mild Alzheimer's disease. *J Nucl Med* 1994;35:1450–1455.
17. Pantano P, Lenzi GL, Guidetti B, et al. Crossed cerebellar diaschisis in patients with cerebral ischemia assessed by SPECT and $^{123}$I-HIPDM. *Eur Neurol* 1987;27:142–148.
18. Perani D, Di Piero V, Lucignani G, et al. Remote effects of subcortical cerebrovascular lesions: a SPECT cerebral perfusion study. *J Cereb Blood Flow Metab* 1988;8:560–567.
19. Perani D, Di Piero V, Vallar G, et al. Technetium-99m-HMPAO SPECT study of regional cerebral perfusion in early Alzheimer's disease. *J Nucl Med* 1988;29:1507–1514.
20. Podreka I, Suess E, Goldenberg G, et al. Initial experience with technetium-99m-HMPAO brain SPECT. *J Nucl Med* 1987;28:1657–1666.
21. Rango M, Candelise L, Perani D, et al. Cortical pathophysiology and clinical neurologic abnormalities in acute cerebral ischemia. A serial study with single-photon emission computed tomography. *Arch Neurol* 1989;46:1318–1322.
22. Rousseaux M, Steinling M, Huglo D, Mazingue A, Barbaste P. Perfusion mapping with $^{99m}$Tc-HMPAO in cerebral hematomas. *J Neurol Neurosurg Psychiatry* 1991;54:1040–1043.
23. Rowe CC, Berkovic SF, Austin MC, et al. Visual and quantitative analysis of interictal SPECT with technetium-99m-HMPAO in temporal lobe epilepsy. *J Nucl Med* 1991;32:1688–1694.
24. Shimosegawa E, Hatazawa J, Inugami A, et al. Cerebral infarction within six hours of onset: prediction of completed infarction with technetium-99m-HMPAO SPECT. *J Nucl Med* 1994;35:1097–1103.
25. Spreafico G, Gadola G, Cammelli F, Caffarra P, Scaglioni A. Semiquantitative assessment of regional cerebral perfusion using $^{99m}$Tc-HMPAO and emission tomography. *Eur J Nucl Med* 1988;14:565–568.
26. Vallar G, Perani D, Cappa SF, Messa C, Lenzi GL, Fazio F. Recovery from aphasia

and neglect after subcortical stroke: neuropsychological and cerebral perfusion study. *J Neurol Neurosurg Psychiatry* 1988;51:1269–1276.
27. Waldemar G, Hasselbalch SG, Andersen AR, et al. Technetium-99m-d,l-HMPAO and SPECT of the brain in normal aging. *J Cereb Blood Flow Metab* 1991;11:508–521.
28. Mountz JM. A method of analysis of SPECT blood flow image data for comparison with computed tomography. *Clin Nucl Med* 1989;14:192–196.
29. Davis SM, Chua MG, Lichtenstein M, Rossiter SC, Binns D, Hopper JL. Cerebral hypoperfusion in stroke prognosis and brain recovery. *Stroke* 1993;24:1691–1696.
30. Hoffman EJ, Cutler PD, Kigby WM, Mazziotta JC. Three-dimensional phantom to simulate cerebral blood flow and metabolic images for PET. *IEEE Trans Nucl Sci* 1990;37:616–620.
31. Hoffman EJ, Cutler PD, Guerrero TM, Digby WM, Mazziotta JC. Assessment of accuracy of PET utilizing a three-dimensional phantom to simulate the activity distribution of [$^{18}$F]fluorodeoxyglucose uptake in the human brain. *J Cereb Blood Flow Metab* 1991;11:A17–A25.
32. Siemens Microdelta User Manual, Revision 1. 1992;13–18.
33. Infeld B, Davis SM, Lichtenstein M, Mitchell PJ, Hopper JL. Crossed cerebellar diaschisis and brain recovery after stroke. *Stroke* 1995;26:90–95.
34. Blokland KA, Reiber HH, Pauwels EK. Quantitative analysis in single-photon emission computed tomography. *Eur J Nucl Med* 1992;19:47–61.
35. Tsui BM, Zhao X, Frey EC, McCartney WH. Quantitative single-photon emission computed tomography: basics and clinical considerations. *Semin Nucl Med* 1994;24: 38–65.
36. King MA, Long DT, Brill AB. SPECT volume quantitation: influence of spatial resolution, source size, shape and voxel size. *Med Phys* 1991;18:1016–1024.
37. Hoffman EJ, Huang SC, Phelps ME. Quantitation in positron emission computed tomography 1. Effect of object size. *J Comput Assist Tomogr* 1979;3:299–308.
38. Williams PL, Warwick R, eds. *Gray's anatomy*, 36th ed. Edinburgh: Churchill Livingstone; 1980:1002–1009.
39. Lenzi GL, Jones T, McKenzie CG, Buckingham PD, Clark JC, Moss S. Study of regional cerebral metabolism and blood flow relationships in man using the method of continuously inhaling oxygen-15 and oxygen-15 labeled carbon dioxide. *J Neurol Neurosurg Psychiatry* 1978;41:1–10.
40. Lenzi GL, Frackowiak RS, Jones T, et al. $CMRO_2$ and CBF by the oxygen-15 inhalation technique. Results in normal volunteers and cerebrovascular patients. *Eur Neurol* 1981;20:285–290.
41. Frackowiak RS, Lenzi GL, Jones T, Heather JD. Quantitative measurement of regional cerebral blood flow and oxygen metabolism in man using $^{15}$O and positron emission tomography: theory, procedure and normal values. *J Comput Assist Tomogr* 1980;4: 727–736.
42. Baron JC, Bousser MG, Comar D, Soussaline F, Castaigne P. Noninvasive tomographic study of cerebral blood flow and oxygen metabolism in vivo. Potentials, limitations and clinical applications in cerebral ischemic disorders. *Eur Neurol* 1981;20:273–284.
43. Devous MD Sr, Stokely EM, Chehabi HH, Bonte FJ. Normal distribution of regional cerebral blood flow measured by dynamic single-photon emission tomography. *J Cereb Blood Flow Metab* 1986;6:95–104.
44. Davis SM, Chua MG, Lichtenstein M, Rossiter SC, Tress BM, Hopper JL. Perfusion changes with recovery after stroke [Abstract]. *Aust N Z J Med* 1993;23:568.
45. Podreka I, Baumgartner C, Suess E, et al. Quantification of regional cerebral blood flow with IMP-SPECT. Reproducibility and clinical relevance of flow values. *Stroke* 1989;20:183–191.
46. Isaka Y, Itoi Y, Imaizumi M, Ashida K, Okamoto M, Iiji O. Quantitation of rCBF by $^{99m}$Tc-hexamethylpropylene amine oxime single-photon emission computed tomography combined with $^{133}$Xe CBF. *J Cereb Blood Flow Metab* 1994;14:353–357.

# Test/Retest Reproducibility of Iodine-123-βCIT SPECT Brain Measurement of Dopamine Transporters in Parkinson's Patients

John P. Seibyl, Kenneth Marek, Kimberly Sheff, Ronald M. Baldwin, Sami Zoghbi, Yolanda Zea-Ponce, Dennis S. Charney, Christopher H. van Dyck, Paul B. Hoffer and Robert B. Innis

*Departments of Diagnostic Radiology, Neurology, and Psychiatry, Yale University School of Medicine, New Haven; and Department of Veterans Affairs Medical Center, West Haven, Connecticut*

Iodine-123-β-CIT has been used as a probe of dopamine transporters in Parkinson's disease patients using SPECT. We studied the test/retest reproducibility of SPECT measures in Parkinson's disease patients and healthy controls obtained after injection of [$^{123}$I]β-CIT in part to assess the utility of this tracer for longitudinal evaluation of striatal dopamine transporters as a marker of disease progression. **Methods:** Seven Parkinson's disease patients and seven healthy control subjects participated in two [$^{123}$I]β-CIT SPECT scans separated by 7–21 days. Subjects were imaged at 24 hr post injection of 360 MBq (9.7 mCi) of [$^{123}$I]β-CIT. Two outcome measures were evaluated; 1) the ratio of specific striatal (activity associated with DA transporter binding) to nondisplaceable uptake, also designated V3," and 2) the total specific striatal uptake (%SSU) expressed as a percentage of injected radiotracer dose. For both measures, test/retest variability was calculated as the absolute difference of test minus retest divided by the mean of test/retest and expressed as a percent. In addition, the reproducibility of left and right striatal asymmetry and putamen:caudate ratios were determined. **Results:** The two outcome measures demonstrated excellent test/retest reproducibility for both the Parkinson's disease and healthy subject groups with variability of striatal V3" = 16.8 ± 13.3% and percent striatal uptake = 6.8 ± 3.4% for Parkinson's disease patients and V3" = 12.8 ± 8.9% and %SSU = 7.0 ± 3.9% for control subjects. There were no statistically significant differences in test/retest variability between control subjects and Parkinson's disease patients for either outcome measure. The reproducibility of left/right asymmetry indices and putamen-to-caudate ratios showed no patient versus control subject differences. The asymmetry index had greater test/retest variability than the other outcome measures. **Conclusion:** These data suggest that SPECT imaging performed at 24 hr postinjection of [$^{123}$I]β-CIT permits calculation of reliable and reproducible measures of dopamine transporters in both Parkinson's disease patients and control subjects and supports the feasibility of using [$^{123}$I]β-CIT in the evaluation of disease progression in Parkinson's disease.

**Key Words:** iodine-123; SPECT; dopamine transporters; Parkinson's disease

**J Nucl Med 1997; 38:1453–1459**

Iodine-123-β-CIT ([$^{123}$I] 2β-carbomethoxy-3β-(4-iodophenyl-tropane) binds with high affinity to dopamine (DA) (IC50 = 1.6 n*M*) and serotonin (IC50 = 3.78 n*M*) transporters and has been used as a SPECT probe in human and nonhuman primates (*1–6*). In baboons, striatal activity is associated with binding to the DA transporters based on dynamic SPECT studies demonstrating displacement of this activity after administration of dopamine transporter-selective, but not serotonin transporter-selective agents (*3*). After intravenous administration of [$^{123}$I]β-CIT in humans, decay-corrected striatal time-activity data showed a prolonged time to highest uptake occurring by 12–18 hr post-tracer injection and very slow rates of striatal washout. Occipital and free parent plasma time-activity data reached a plateau earlier than striatum and also demonstrated extremely

Received July 3, 1996; revision accepted Jan. 20, 1997.

For correspondence or reprints contact: John P. Seibyl, MD, Section of Nuclear Medicine, TE-2 Department of Diagnostic Radiology, Yale University School of Medicine, 333 Cedar St., New Haven, CT 06510.